Interface amorphization: a molecular dynamics approach

1994 J. Phys.: Condens. Matter 6 4213

(http://iopscience.iop.org/0953-8984/6/23/001)

J. Phys.: Condens. Matter 6 (1994) 4213–4224. Printed in the UK

Interface amorphization: a molecular dynamics approach

Sebastián Gonçalves†, Ricardo Ramírez‡ and Miguel Kiwi‡

† Instituto de Física, Universidade Federal do Rio Grande do Sul, CP 15051, 91501-570 Porto Alegre, Brazil

‡ Facultad de Física, Universidad Católica de Chile, Casilla 306, Santiago 22, Chile

Received 24 January 1994

Abstract. A two-dimensional molecular dynamics model is introduced in order to obtain a better understanding of interface amorphization. We start from a monodisperse system of particles arranged on a perfect two-dimensional triangular lattice, which is divided into two separate regions. In one of these regions the particle size is uniformly reduced, while in the other it is enlarged, preserving the total system 'volume'. Using a whole wealth of diagnostic tools, and visualizations of the particle distributions, a clear distinction between the bulk and the interface disordering transition emerges. Several interesting phenomena, such as the formation of defects, hysteresis of the transition, single-layer displacement and grain boundary development in the vicinity of the interface, show up in our simulations.

1. Introduction

It is well known that interest in the physics of interfaces has increased during the last decade. Multilayers, thin films and surfaces have been studied experimentally, theoretically and by means of numerical simulations. The cause for this interest is the vast number of novel and exciting properties that these systems exhibit. Due to two factors, their effective low dimensionality—the relevant physics of an interface is essentially two-dimensional (2D)—and the availability of superlattices with unusually large lattice parameters, experimentalists have found a rich new world of electronic and magnetic properties, which in the past was restricted only to theoretical fancy [1]. The giant magnetoresistance of metallic superlattices, such as Fe–Cr [2], discovered a few years ago, is a good example.

However, in shaping such systems, structural considerations have to be taken into account. For example, depending on the types of atom present at either side of the interface, it can adopt an ordered structure or an amorphous configuration [3]. This spatial distribution of atoms has important implications for their electronic and magnetic properties, and for their technological applications.

In a recent paper Bocquet *et al* [4] using molecular dynamics (MD) at constant temperature, obtained a first-order phase transition in a 2D substitutional binary alloy. Following a closely related procedure we carry out an MD study to investigate the order–disorder transition of a simple 2D system with an interface, whose results we report in this contribution.

Our system, which is represented in figure 1, can be described as follows: a large number of discs, regularly arranged on an area bounded by a hexagon and subject to periodic boundary conditions, interact via a repulsive potential. The existence of an interface is induced by slowly increasing the atomic diameter of a cluster of discs, while reducing the size of the rest, preserving the total 'volume' of the system. In doing so we simulate, via

0953-8984/94/234213+12$19.50

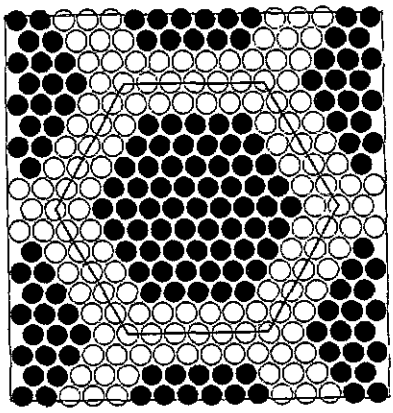

Figure 1. Starting configuration ($T = 0$ and $\lambda = 1$) of the $N = 108$-particle system. The hexagon, which contains 47 empty and 61 filled discs, is repeated periodically to generate the system. Later on the filled (empty) discs are allowed to decrease (increase) in size.

MD, the time evolution of the system, while keeping constant the volume, the average atomic diameter (system size) and the temperature. The change in diameter of the discs has to be carried through in steps small enough to guarantee, as far as it is feasible with presently available computational resources, that the system is always in quasi-static thermodynamic equilibrium.

As the above described process is carried through we evaluate several order parameters, that allow us to probe and characterize the degree of order of the system, and in particular of the interface. This way we find the critical atomic size ratio that generates a phase transition, from the initially ordered crystal, to a disordered structure with an amorphous interface. The procedure just described is carried out for several different configurations and temperatures.

This paper is organized as follows. In section 2 we specify analytically the model and the dynamics we have employed to simulate its time evolution. Section 3 is devoted to the definition and discussion of the order parameters used for the diagnostics. In section 4 we provide and analyse the results obtained in our computations. The conclusions are finally presented in section 5.

2. Model

Following Bocquet *et al* [4] we consider a 2D model, in which a fixed number of 'soft discs' interact through a purely repulsive pair potential, given by

$$V_{\alpha\beta} = \epsilon \left(\frac{\sigma_{\alpha\beta}}{r}\right)^{12} \tag{2.1}$$

where ϵ sets the energy scale and r is the distance between centres of a pair of interacting discs. $\sigma_{\alpha\beta}$ is the distance between two discs in contact, and is defined by

$$\sigma_{\alpha\beta} = \tfrac{1}{2}(\sigma_\alpha + \sigma_\beta) \qquad 1 \leqslant \alpha, \beta \leqslant 2. \tag{2.2}$$

In our computations we start with a hexagon that accommodates N close packed discs arranged on a perfect triangular lattice. Next the system is divided into two regions, as

illustrated in figure 1. In one of the regions the diameter of N_1 of the discs is dilated, while at the same time the rest of them ($N_2 \equiv N - N_1$) shrink, keeping constant a mean atomic diameter σ to be defined later on.

The size ratio of the two species of particle in the system is denoted by the parameter

$$\lambda = \frac{\sigma_1}{\sigma_2} \leqslant 1 \tag{2.3}$$

and the concentration of each of the species is given by $x_i = N_i/N$.

A dimensionless coupling constant γ is now introduced as

$$\gamma = \frac{N\sigma^2}{\Omega}\left(\frac{\epsilon}{k_B T}\right)^{1/6}. \tag{2.4}$$

Here $N\sigma^2/\Omega$ and $k_B T/\epsilon$ play the role of reduced number density and temperature, respectively. The size ratio λ, the concentrations x_i and the non-dimensional coupling constant γ, fully specify the equilibrium thermodynamic properties of the system [5].

As mentioned above, our simulations were carried out starting with a monodisperse system, characterized by $\lambda = 1$, and little by little reducing the size ratio to $\lambda < 1$ values. In doing so conformal solution theory [6] is used, which allows to define the mean diameter σ by the constraint

$$\sigma^2 = x_1^2\sigma_{11}^2 + 2x_1x_2\sigma_{12}^2 + x_2^2\sigma_{22}^2. \tag{2.5}$$

For our simulations the natural MD time unit is $\tau = \sqrt{m\Omega/N\epsilon}$, where m is the mass of the particles, and the time step we adopted was $\Delta t = 5 \times 10^{-3}\tau$. All our simulations were carried out for a constant number of each type of particle N_i; thus, the density also remained fixed. The temperature was held constant by means of the thermostat of Hoover *et al* [7] in the version due to Brown and Clarke [8]. Consequently, on the basis of the arguments given after (2.4), all of our numerical results correspond to a fixed value of γ, while λ is the sole free parameter.

As mentioned above, the reduction of the size ratio λ was performed in a sequence of tiny steps. We adopted the value $\delta\lambda = 10^{-5}$ followed by constant λ stabilization periods of 400 time steps Δt. After a transient stabilization period elapsed, the statistical averages reported below were taken over $2000\Delta t$, every $\Delta\lambda = 500\delta\lambda$.

An exception to the above is made for the specific case of figure 7(a) and 7(b), where after reducing λ we also proceed to increase its value back to $\lambda = 1$, in order to evaluate hysteresis effects near the critical size ratio. In this case we allow the system to relax for $2000\Delta t$ after every modification $\delta\lambda$, and we compute the order parameters every $\Delta\lambda = 100\delta\lambda$.

3. Order parameters

As the interface is created, by modification of the monodisperse ($\lambda = 1$) initial condition, the system evolves from a perfect crystal towards a binary configuration with a certain degree of disorder, which eventually leads to a phase transition. As this develops, and in addition to the customary visualizations and phase diagrams, five types of order parameter are used in this paper to monitor and characterize the order–disorder transition [4]. They are defined as follows:

(i) The structure factor, which is a measure of the translational order,

$$\rho_G = \left\langle \frac{1}{N} \left| \sum_i \exp(i\boldsymbol{G}\cdot\boldsymbol{R}_i) \right| \right\rangle \tag{3.1}$$

where $\boldsymbol{R}_i$ specifies the position of atom i and N is the total number of atoms in the system. Here and throughout $\langle \ldots \rangle$ denotes the ensemble average. ρ_G is evaluated for a specific reciprocal lattice vector $\boldsymbol{G}$ of the triangular lattice. The structure factor becomes $\rho_G = 1$ for a perfectly ordered periodic lattice, and decreases as $1/\sqrt{N}$ when complete disorder sets in.

(ii) Another way to measure the degree of translational order is the mean square displacement $\langle \Delta r \rangle^2$, given by

$$\langle \Delta r \rangle^2 = \frac{1}{N} \sum_{i=1}^{N} \langle (\boldsymbol{R}_i - \boldsymbol{R}_{i0})^2 \rangle \tag{3.2}$$

where $\boldsymbol{R}_{i0}$ specifies the lattice position of atom i. Thus, $\langle \Delta r \rangle^2$ is a measure of the displacement of the atoms from their zero-temperature equilibrium positions.

(iii) The bond orientation order is probed through the Nelson–Halperin [9] order parameter

$$\langle \Psi_{ij} \rangle = \frac{1}{N} \sum_{i=1}^{N} \left\langle \left| \frac{1}{n_i} \sum_{j=1}^{n_i} e^{i6\theta_{ij}} \right| \right\rangle \tag{3.3}$$

where n_i is the number of nearest neighbours of atom i and θ_{ij} is the angle formed by the bonds of an (i, j) pair of nearest neighbours. $\langle \Psi \rangle$ is unity for a perfect triangular crystal, and tends towards zero as the structure disorders locally.

(iv) Along the same lines we computed the fraction f_6 of atoms having exactly six neighbours, counting the number of particles within a cut-off radius r_c lying midway between nearest and next-nearest lattice positions, and given by

$$f_6 = \frac{1}{N} \left\langle \sum_{i=1}^{N} \delta_{n_i,6} \right\rangle. \tag{3.4}$$

This method is much easier and faster than using the Voronoï construction and has been shown to be equivalent to it within 1% at least for the dense fluid phase near freezing and in the solid phase [10].

As the system consists of two well defined clusters, we compute separately for each one of them the order parameters presented above. This way ρ_G^i denotes the ρ_G order parameter evaluated over the cluster of atoms of species i ($i = 1, 2$). The same is valid for the $\langle \Delta r \rangle^2$ order parameter. For the Nelson–Halperin [9] order parameter we make a distinction between three types of bond: $\langle \Psi_{11} \rangle$ for bonds between type 1 atoms, $\langle \Psi_{22} \rangle$ between type 2 atoms and $\langle \Psi_{12} \rangle$ for mixed bonds. The latter evaluates the degree of order at the interface between the two clusters. f_6^i is evaluated over the cluster i, independently of the kind of neighbour the particle actually has.

(v) The g_{ij} pair correlation functions where i and j, in this particular case, assume the values 1 and 2 to label the smaller and larger than average discs, respectively. Analytically it is defined by

$$g_{ij} = \frac{\Omega}{N^2} \left\langle \sum_i \sum_{j \neq i} \delta(\boldsymbol{R} - \boldsymbol{R}_{ij}) \right\rangle \tag{3.5}$$

where Ω is the 'volume' (in our case actually the area) of the system.

In addition to the above defined order parameters, the diagnostics are complemented with illustrative visualizations of averaged atomic position, pressure versus atomic size ratio λ, and coupling constant γ versus λ phase diagrams.

4. Numerical results

In this section we report the results of our numerical computation, obtained following the scheme outlined above. Basically we adopted the value $N = 108$ for the number of particles in our system; however, some runs for a system of quadruple size, i.e. $N = 432$, were also performed to check on size effects. The latter number of particles essentially corresponds to the largest that can be handled with present day computers, within reasonable machine times.

The choice of N is a non-trivial matter, since it has to be consistent with the boundary conditions imposed on the system. The exterior hexagonal boundary is consistent with $N = 108$, but it severely restricts the choice of N_1, the number of particles in the smaller internal hexagon of figure 1, particularly if one demands that the concentrations $x_i \simeq \frac{1}{2}$. Actually, we have adopted $N_1 = 61$, which implies $x_1 \cong 0.5648$.

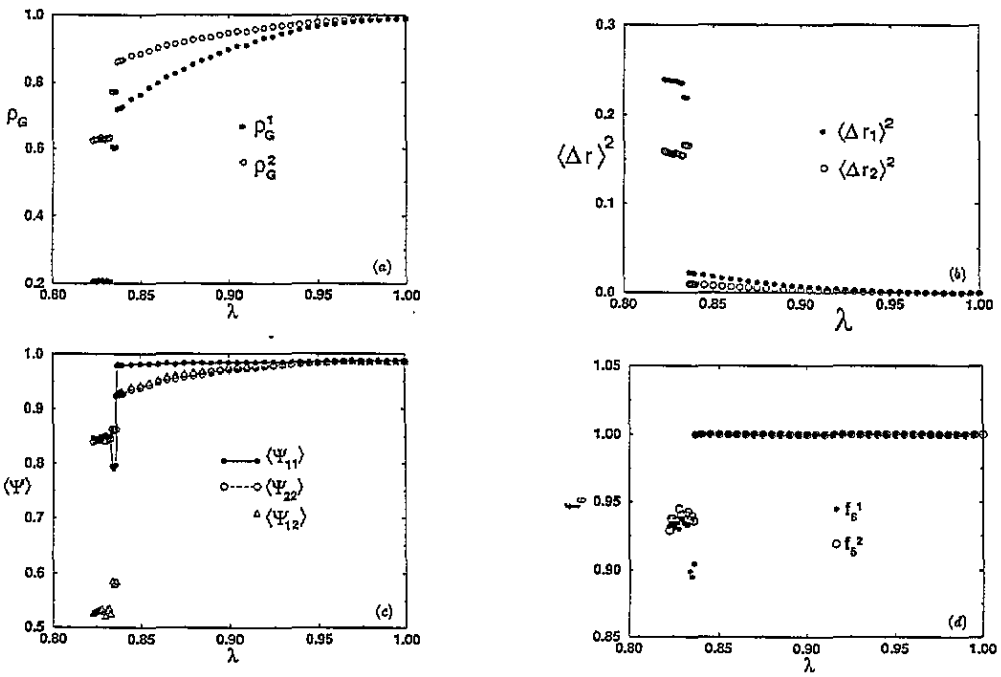

Figure 2. Order parameters versus size ratio λ for a constant value of the coupling constant $\gamma = 1.64$. (a) Structure factor ρ_G; (b) mean square displacement $\langle \Delta r \rangle^2$; (c) Nelson–Halperin order parameter $\langle \Psi \rangle$ and (d) fraction of atoms having exactly six neighbours f_6.

In figure 2 we present plots of the structure factor ρ_G, the mean square displacement $\langle \Delta r \rangle^2$, the bond orientation parameter $\langle \Psi \rangle$ and the fraction of atoms having exactly six neighbours f_6, versus the size ratio λ. All of them correspond to $\gamma = 1.64$. The four plots

provide consistent and complementary information on the behaviour of the system and the phase transition it undergoes. In fact, all of them show a sharp phase transition occurring in a narrow region around the critical value $\lambda_c = 0.835$.

The structure factor, plotted in figure 2(a), indicates that the interior smaller-diameter particles lose translational order at a faster rate than the exterior dilated-diameter ones. It is also apparent that a few metastable states are reached in the vicinity of the transition; their small number is certainly due to the relatively limited system size. These metastable states, and the $\lambda < 0.83$ stable configurations, exhibit a degree of translational order which depends significantly on whether one considers the smaller- or larger-particle-diameter regions.

The mean square displacement parameter, illustrated in figure 2(b), also provides a clear cut notion of what goes on, with a sharp discontinuity at the phase transition, and metastable states in its vicinity. However, the bond orientation parameter (figure 2(c)) evidences two special features: it is the only parameter in these figures which probes interfacial disorder, and it exhibits a qualitatively different behaviour from the rest. In fact, in the smaller-particle region the value of $\langle \Psi_{11} \rangle$ remains quite constant, while both $\langle \Psi_{22} \rangle$ and $\langle \Psi_{12} \rangle$ show a quite disparate alteration of their magnitude. The similar trends of $\langle \Psi_{22} \rangle$ and $\langle \Psi_{12} \rangle$ break down below the transition, with the interfacial bond order showing a manifestly larger change (37% as compared with 6%). Possibly this large variation is the clearest indication of a qualitative change at the interface. This can easily be understood on the basis of a simple physical picture: the interior region shrinks preserving the hexagonal geometry and, to a certain degree, so does the exterior region, but not the interface which suffers major strains in the adjustment process. This all seems to indicate that, after undergoing the disordering transition, the particles in the interior and exterior regions find a way to achieve local bulk order, but find it hard to adjust at the interface.

The main features of the preceding figures are consistent with the behaviour of f_6^i, displayed in figure 2(d). The unique characteristic of this orientational order parameter is the constant value it adopts ($f_6^i = 1$, independent of i) all the way to the phase transition which occurs at $\lambda_c \cong 0.835$. However, when compared with the rest of the order parameters, it suffers the smallest change (of only 7%) at the phase transition, if the metastable values of $f_6^1 \cong 0.9$ are ignored.

The pair correlation functions g_{11}, g_{22} and g_{12} are plotted in figure 3(a), (b) and (c), respectively. Our first observation is that these plots are consistent with a phase transition around $\lambda \cong 0.837$. Moreover, it is noticed that the peaks of g_{11} correspond to a triangular lattice that has shrunk, while those of g_{22} correspond to the expected expanded lattice. It is also worth mentioning that, to a large extent, the structure is lost for $\lambda \cong 0.836$.

For our purposes the most interesting of the pair correlation functions is g_{12}, which provides an insight into the interfacial structure. In fact, before the bulk transition takes place, i.e. for $\lambda \leqslant 0.837$, plenty of structure is observed, which is due to pairs of atoms belonging to different sets (interior and exterior), each of them with different distance parameters. This structure disappears below the phase transition, when a liquid-like structure pair correlation function seems to emerge, suggesting the presence of interfacial amorphization.

Pictures are always quite eloquent. Thus, here and throughout, we provide images of the average particle position. Figure 4 portrays the particles just above $\lambda > \lambda_c$ (figure 4(a)), in the metastable region $\lambda \cong \lambda_c$ (figure 4(b)), and just below $\lambda < \lambda_c$ (figure 4(c)), the phase transition. While it is apparent that a degree of long- and short-range order is preserved as the system undergoes the transition, we observe that the latter gives rise to plenty of defects, especially in the neighbourhood of the interface. Moreover, the critical fluctuations

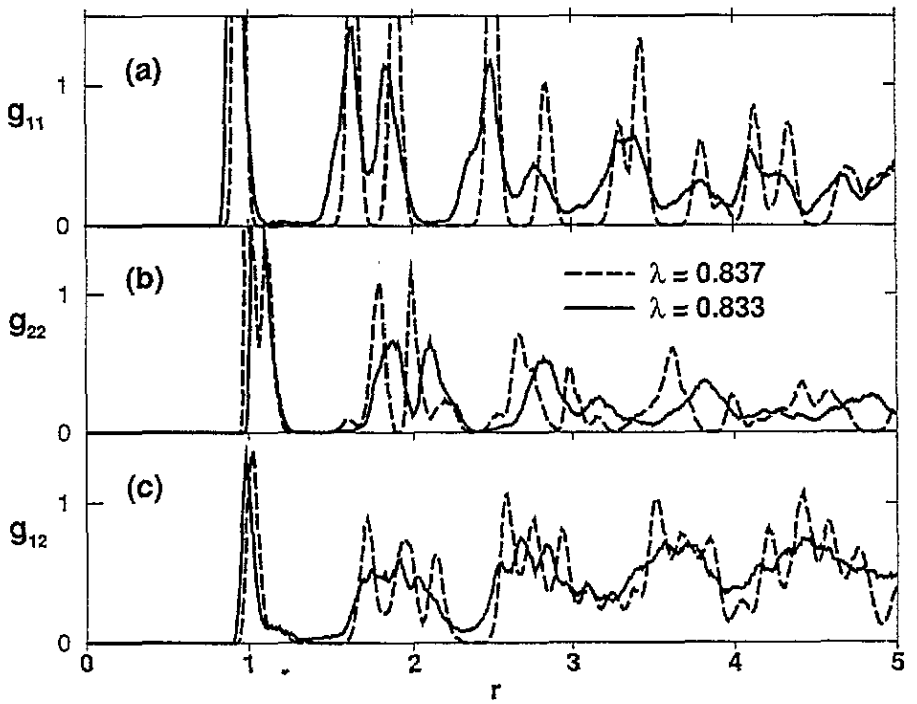

Figure 3. Pair correlation functions $g(r)$ just before ($\lambda = 0.837$), and after ($\lambda = 0.833$), the disordering transition, as a function of radial distance on the plane r, in units of triangular lattice spacing.

observed in figure 4b are quite remarkable. In addition, the simulations below λ_c verify that some local order is recovered, once the critical fluctuations near the transition are quenched.

In figure 5 the pressure p versus size ratio λ plot reinforces the notion of a sharp first phase transition. No trace of the presence of metastable states appears, thus hinting that these states are of nearly equal energy, since pressure and free energy differ only by a constant factor.

General trends to illustrate the influence of the magnitude of the coupling constant are displayed in figure 6, by means of a phase diagram for the order–disorder transition in the λ–γ plane. It is observed that order emerges only when the coupling strength $\gamma \geqslant 1$, but, after order sets in, it is stable practically up to the critical value λ_c.

To better understand the transition, and to add a more dynamical point of view, we also investigated its hysteresis. In figure 7 we show results for the interfacial bond orientation order parameter $\langle \Psi_{12} \rangle$, obtained by first shrinking and then expanding the size ratio λ. Of special interest is the re-crystallization process that is observed in figure 7(a) as λ grows above 0.83. As expected, the re-crystallization trajectory is not as sharp as the disordering transition but, after the intermediate region $0.835 < \lambda < 0.865$ is crossed, the full magnitude of the order parameter is recovered. This indicates that the initial ordered configuration is fully regained.

On the other hand, if the reduction of λ is stopped at 0.83, as illustrated in figure 7(b), then the original value of $\langle \Psi_{12}(\lambda = 1) = 1 \rangle$ is recovered only asymptotically. This strongly suggests the presence of defects, even in the monodisperse $\lambda = 1$ limit; to find out if this is the case we examine a snapshot of the average configuration (figure 7(c)) in this $\lambda = 1$ limit.

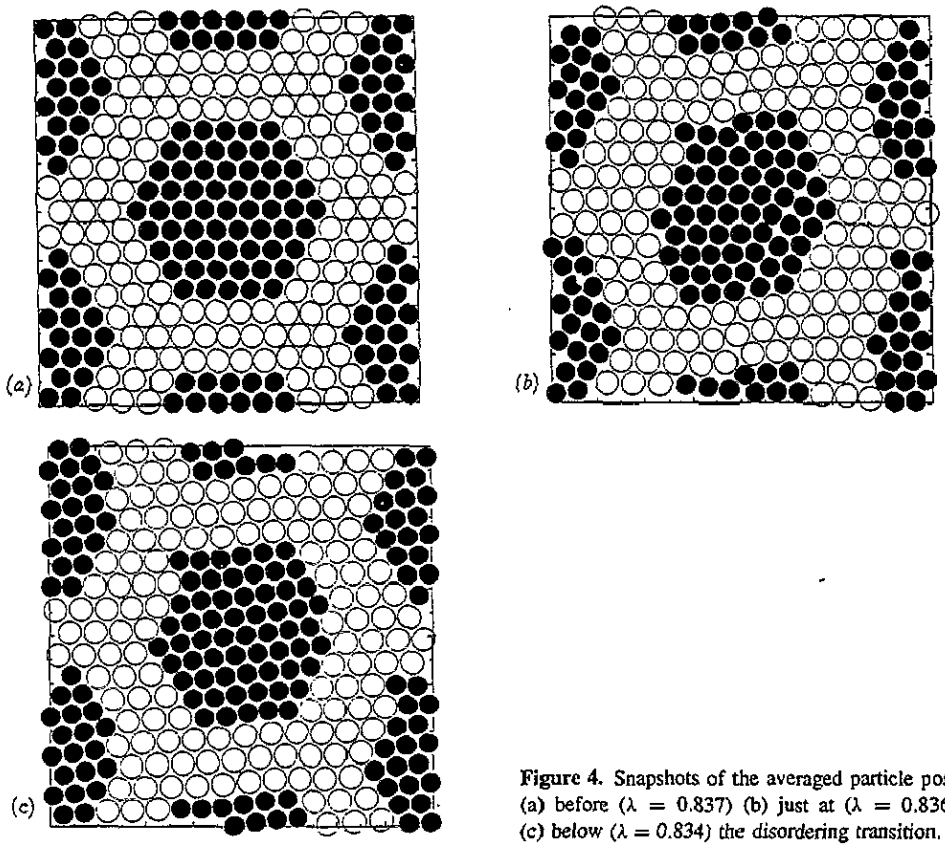

Figure 4. Snapshots of the averaged particle positions (a) before ($\lambda = 0.837$) (b) just at ($\lambda = 0.836$) and (c) below ($\lambda = 0.834$) the disordering transition.

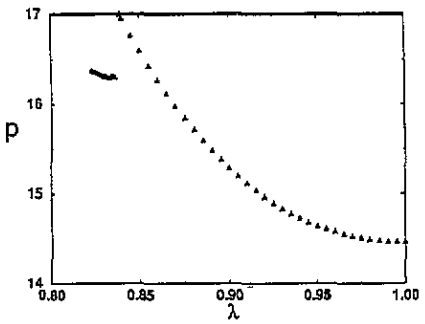

Figure 5. Pressure p, in units of ϵd_{NN}^2 (where d_{NN} is the triangular lattice spacing) versus size ratio λ.

While most atoms are aligned and have six first-nearest neighbours, with 60° bond angles, a hole is present barring the system from recovering its full original symmetry. The existence of a hole implies a non-uniform increased density around it. Also due to the presence of the hole, there is an energy barrier that has to be surmounted to recover the perfect symmetry configuration; so to say, the hole locks the particles in place, into a squeezed environment, without allowing the neighbours to occupy the void. Obviously, if this flawed system is subject to an annealing process the perfect original configuration is recovered.

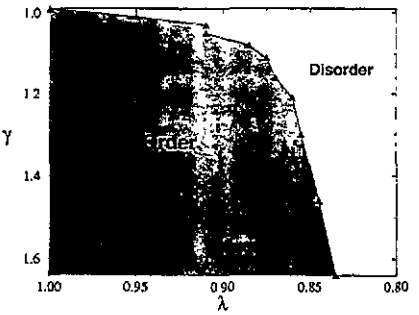

Figure 6. Phase diagram for the order–disorder transition in the λ–γ plane. Notice the decreasing scale of both the λ and the γ axis.

A complementary understanding is obtained by the examination of figure 7(d), which provides a plot of pressure versus λ. It should be noticed that pressure and Helmholtz free energy, in our case where the potential obeys a simple power law, differ only by a constant factor, and thus we will take them to be essentially equivalent. We observe that, for decreasing λ, the transition is easily distinguished by a pressure (free energy) discontinuity. Subsequent minor changes in the order parameters are not perceived in the free energy plot, since they correspond to transitions between states of practically the same energy. On the contrary, for increasing λ the curve is smooth, and a crossing with the decreasing trajectory occurs for $\lambda = 0.875$, which signals the coexistence, in thermodynamic equilibrium, of the ordered and disordered phases. However, there is no transition from one to the other, since an energy barrier of unknown height separates them: thus, hysteresis is present in this first-order phase transition.

This way, during our simulations, the system can adopt an energy-wise unfavourable metastable disordered configuration all the way up to the monodisperse limit $\lambda = 1$, due to the fact that the energy barrier cannot be surmounted within the amount of time available for computation. This points towards two shortcomings of these simulations: (i) the short time that is feasible to carry them out; and (ii) the finite size of the system. It is expected that the energy barrier associated with a single vacancy will become smaller as the size of the sample increases, thus reducing the likelihood for a vacancy to survive in a homogeneous system.

Finally, we also have tried to assess the effects of finite size through an example: enlarging the system from 108 to 432 particles. In figure 8 we plot versus λ, the bond orientation order parameter $\langle \Psi_{ij} \rangle$ which is the most sensitive one to interfacial disorder, and which ought to be compared with figure 2(c). While the same qualitative behaviour is observed in these two figures, the transition is slightly displaced, from $\lambda \cong 0.835$ in figure 2(c), to $\lambda \cong 0.860$ in the present case. We ascribe the difference to the change in concentration of smaller particles, from $x_1 = 61/108 \cong 0.5648$, to $x_1 = 215/432 \cong 0.4977$ (we recall the comment, made in relation to figure 1, pointing out the restriction imposed by geometry on the choice of N_1, the number of particles inside the interior hexagon). In general, it is to be expected that the smaller the value of x_1, the more unstable the system is, and the sooner the transition takes place.

Another quantitative difference is the extents of the discontinuity of $\langle \Psi_{11} \rangle$ and $\langle \Psi_{22} \rangle$, which were of between 10% and 20% for the 108-particle system, and are of less than 5% now, for the 432-particle system. This is a size effect, since now the number of atoms barely affected by the interface is much larger and they are less influenced by the transition.

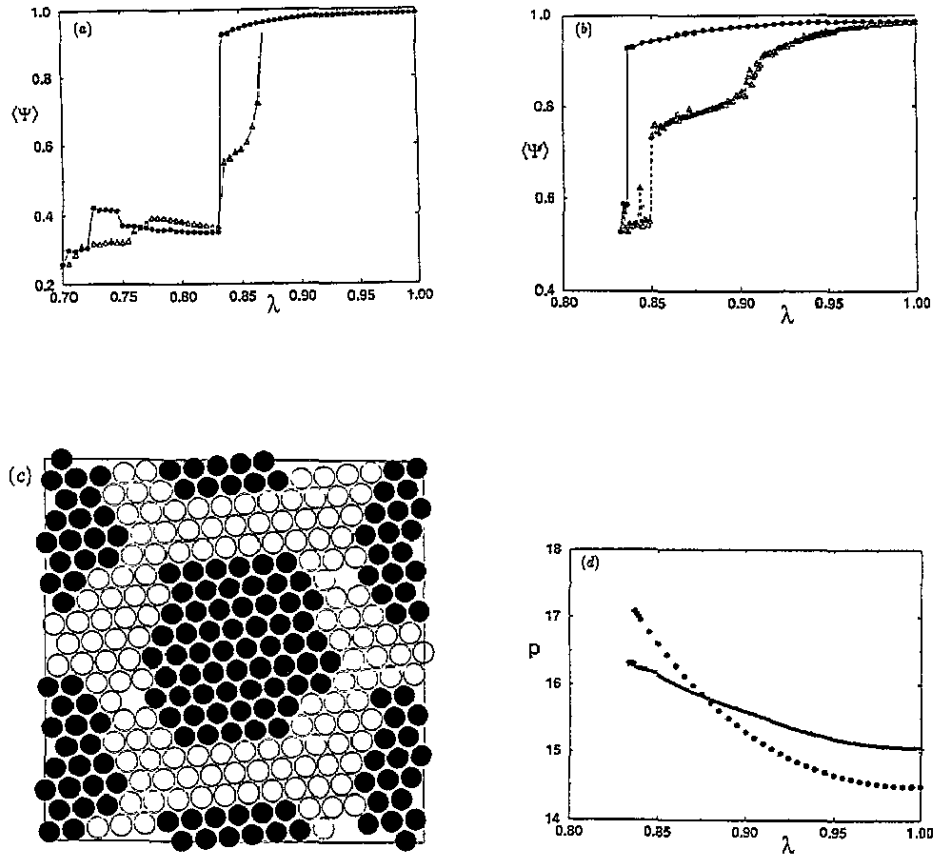

Figure 7. The hysteresis of the process. (a) Interfacial bond order parameter $\langle\Psi_{12}\rangle$ for λ shrinking to 0.7 (filled circles) and then expanding back to unity (open triangles); (b) as (a) but stopping at $\lambda = 0.83$ (filled circles) and expanding back to unity (open triangles); (c) snapshot of average particle positions after process (b), for $\lambda = 1$; (d) pressure p (free energy) versus λ, corresponding to the process illustrated in (b).

Actually, in the infinite-size limit $\langle\Psi_{11}\rangle$ and $\langle\Psi_{22}\rangle$ should be continuous at the transition, which only would be reflected in the $\langle\Psi_{12}\rangle$ order parameter. In fact, the latter retains the magnitude of the discontinuity, which provides us with reassurance on the soundness of our inferences.

In figure 9 we provide a picture of the particle positions for $\lambda = 0.855$, just after the transition. As expected, the richness of defects is now quite apparent. While before, in figure 7(c), displaced and five nearest-neighbour atoms could be seen, we now observe, in addition to those defects, the displacement of single layers, and the emergence of a grain boundary at the lower interface region.

5. Summary and conclusion

In this contribution we have used the molecular dynamics (MD) model introduced by Bocquet *et al* [4] to study the bulk amorphization process, in order to shed light on interface

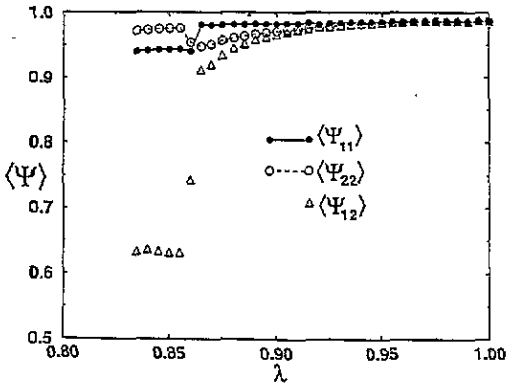

Figure 8. Bond orientation order parameter $\langle \Psi_{ij} \rangle$ versus λ, for a 432-particle system. This plot is to be contrasted with figure 2(c).

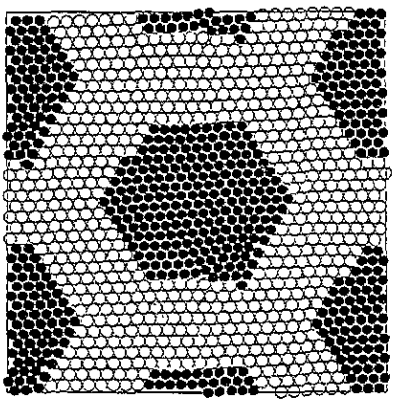

Figure 9. Snapshot of the larger ($N = 432$) system, for $\lambda = 0.855$, which illustrates the nature and the richness of the defect structure.

amorphization. To do so we have shrunk (or eventually enlarged) the radii of the particles in a region of space, bound by an hexagonal border. This differs from [4] where the particle radii were shrunk or enlarged at random. On this basis we have been able to show that the discontinuous transition from a 2D crystal to an amorphous solid has special and quite interesting characteristics at the interface that we create in our simulations.

In fact, the disordering process is more marked at the interface, especially when the bond orientation order parameter $\langle \Psi_{12} \rangle$ and the number of nearest neighbours f_6^i are used as visualization criteria. Moreover, layer displacements, a high density of defects and precursors of grain boundary nucleation, in the vicinity of the interface, are also observed in our simulations. These phenomena are quite different from, and should not be confused with, the melting transition which occurs at higher temperatures.

Due to the relatively small number of particles in the system, some energetically unfavourable metastable states are generated; moreover, they sometimes induce hysteretic effects. These states cannot be eliminated within available computing times, but they can be qualitatively understood through the examination of pictures of the particle distribution

in our system.

In summary, we have been able to produce a simple MD model which allows us to obtain some insight into the interface amorphization phenomenon, hinting to classical size effects as the main driving mechanism.

Acknowledgments

We gratefully acknowledge stimulating conversations with Dr Mariana Weissmann. This work has been supported by the Fondo Nacional de Investigaciones Científicas y Tecnológicas (FONDECYT, Chile) and the Fundación Andes. One of us (SG) would like to acknowledge the support of FAPERGS (Fundação de Amparo à Pesquisa do Estado do Rio Grande do Sul, Brazil).

References

[1] Ando T, Fowler A B and Stern F 1982 *Rev. Mod. Phys.* **54** 437
[2] Baibich M N, Broto J M, Fert A, Nguyen Van Dau F, Petroff F, Etienne P, Creuzet G, Friederich A and Chazelas J 1988 *Phys. Rev. Lett.* **61** 2472
[3] Weissmann M, Ramírez R and Kiwi M 1992 *Phys. Rev.* B **46** 2577
[4] Bocquet L, Hansen J P, Biben T and Madden P 1992 *J. Phys.: Condens. Matter* **4** 2375
[5] Hoover W G, Ross M, Johnson K W, Henderson D, Baker J A and Brown B C 1970 *J. Chem. Phys.* **52** 4931
[6] Leland T W, Rowlinson J S and Sather G A 1968 *Trans. Faraday Soc.* **64** 1447
[7] Hoover W G, Ladd and Moran 1982 *Phys. Rev. Lett.* **48** 1818
[8] Brown and Clarke 1984 *Mol. Phys.* **51** 1243
[9] Nelson D R and Halperin B I 1980 *Phys. Rev.* B **21** 5312
[10] Broughton J Q, Gilmer G H and Weeks J D 1982 *Phys. Rev.* B **25** 4651